GNSS L5/E5 Maximum Likelihood Synchronization Performance Degradation under DME Interferences

Lorenzo Ortega
IPSA Toulouse/TéSA
Toulouse, France
lorenzo.ortega@ipsa.fr

Corentin Lubeigt
TéSA/ISAE-Supaero
Toulouse, France
corentin.lubeigt@tesa.prd.fr

Jordi Vilà-Valls
ISAE-Supaero
Toulouse, France
jordi.vila-valls@isae-supaero.fr

Eric Chaumette
ISAE-Supaero
Toulouse, France
eric.chaumette@isae-supaero.fr

***Abstract*—Global Navigation Satellite Systems (GNSS) are a key player in a plethora of applications. For navigation purposes, interference scenarios are among the most challenging operation conditions, which clearly impact the maximum likelihood estimates (MLE) of the signal synchronization parameters. While several interference mitigation techniques exist, a theoretical analysis on the GNSS MLE performance degradation under interference, being fundamental for system/receiver design, is a missing tool. The main goal of this contribution is to introduce a mathematical tool to evalute the effect of any type of interference on any GNSS signal. Regarding such tool, we provide closed-form expressions of the misspecified Cramér-Rao (MCRB) bound and estimation bias, for a generic GNSS signal corrupted by an interference. The proposed expressions are used to analyze the GNSS performance degradation induced by the distance measuring equipment (DME) system.**

***Index Terms*—GNSS synchronization, DME interference, maximum likelihood, misspecified CRB, bias analysis.**

I. Introduction

Global Navigation Satellite Systems (GNSS) [1] appear in a plethora of applications, ranging from navigation and timing, to Earth observation, attitude estimation or space weather characterization. Indeed, reliable position, navigation and timing information is fundamental in new application such as intelligent transportation systems or autonomous unmanned ground/air vehicles, for which GNSS have become the cornerstone source of positioning data, and this dependence can only but grow in the future. But GNSS were originally designed to operate in clear sky nominal conditions, and their performance clearly degrades under harsh environments. Among the non-nominal operation conditions, multipath, spoofing and interferences (i.e., intentional or unintentional) are the most challenging ones, being a key issue in safety-critical scenarios [2]. It is well known that interferences may degrade GNSS performance. These effects have been reported in the state-of-the-art, and several interference mitigation countermeasures have already been proposed [3]–[7]. A particular type of interference, of interest in the aviation domain, is the one caused by distance measuring equipment (DME) and tactical air navigation (TACAN) systems.

Indeed, these systems transmit at the aeronautical radionavigation services band, which overlaps the GNSS E5 band [8]. From an estimation point of view, it is important to theoretically analyze how different interferences degrade the GNSS synchronization performance, that is, the delay and Doppler estimation stage of the GNSS receiver. Because the optimal solution is given by the maximum likelihood estimator (MLE), it is sound to obtain the corresponding Cramér-Rao bound (CRB). Note that the CRB gives an accurate estimation of the mean square error (MSE) of the MLE in the asymptotic region of operation, i.e., in the large sample and/or high signal-to-noise (SNR) regimes of the Gaussian conditional signal model (CSM) [9]. Several CRBs for different GNSS receiver architectures operating under nominal conditions are available in the literature [10]. In addition, in recent papers closed-form CRBs under non-nominal conditions (e.g. multipath [11], acceleration systems [12]) have been derived. In this contribution, we provide a mathematical tool that allows to characterize the performance degradation induced by an interference at the first GNSS receiver stages. The main hypothesis is that the receiver is not aware that an interference is present, and therefore, it assumes that the received signal is only corrupted by additive Gaussian noise. This implies that the signal model at the receiver input and the assumed signal model do not coincide, that is, there exists a model mismatch [13]. In that case, the MLE is no longer unbiased, and one needs to obtain: i) the estimation of the bias induced by the interference [14], and ii) the corresponding misspecified CRB (MCRB) [15].

The goal of this contribution is twofold: 1) to introduce to the GNSS community how this new tool can be used in order to evaluate the effect of any kind of interference on any GNSS signal, at the receiver synchronization step, and, as an example of interest, 2) to analyze the performance degradation induced by a DME interference on GNSS signals within the L5 band. The analysis provided in this article allows to assess, for instance, which is the maximum acceptable signal to noise+interference power ratio for a correct receiver operation, or the expected synchronization performance under different interference powers. A set of simulation results for the DME interference and GNSS signals in the L5/E5a band are provided to support the discussion.

II. True and Misspecified Signal Models

A. Correctly Specified Signal Model

A GNSS band-limited signal $s(t)$, with bandwidth B, is transmitted over a carrier frequency f_c ($\lambda_c = c/f_c$, $\omega_c = 2\pi f_c$). The synchronization parameters to be estimated are the

delay and Doppler shift, $\boldsymbol{\eta} = (\tau, b)^\top$. Under the narroband assumption, the influence of the Doppler parameter on the baseband signal samples is negligible, $s((1-b)(t-\tau)) \approx s(t-\tau)$ [16]. For short observation times, a good approximation of the baseband output of the receiver's Hilbert filter (GNSS signal + interference) is [17],

$$x\left(t;\boldsymbol{\eta}\right) = \alpha s\left(t-\tau\right) e^{-j2\pi f_c(b(t-\tau))} + I(t) + n\left(t\right), \quad (1)$$

with $I(t)$ a band-limited unknown interference within the frequency band of interest, $n(t)$ a complex white Gaussian noise with unknown variance σ_n^2 and α a complex gain. The discrete vector signal model is built from $N = N_1 - N_2 + 1$ samples at $T_s = 1/F_s = 1/B$,

$$\mathbf{x} = \alpha \mathbf{a}(\boldsymbol{\eta}) + \mathbf{n} = \rho e^{j\Phi}\mathbf{a}(\boldsymbol{\eta}) + \mathbf{n} = \alpha \boldsymbol{\mu}(\boldsymbol{\eta}) + \mathbf{I} + \mathbf{n}, \quad (2)$$

with $\mathbf{x} = (\ldots, x\left(kT_s\right), \ldots)^\top$, $\mathbf{I} = (\ldots, I\left(kT_s\right), \ldots)^\top$, $\mathbf{n} = (\ldots, n\left(kT_s\right), \ldots)^\top$, $N_1 \leq k \leq N_2$ signal samples, and

$$\mathbf{a}(\boldsymbol{\eta}) = (\ldots, s(kT_s - \tau)e^{-j2\pi f_c(b(kT_s-\tau)} + \frac{1}{\alpha} I(kT_s) \ldots.)^\top, \quad (3)$$

$$\boldsymbol{\mu}(\boldsymbol{\eta}) = (\ldots, s(kT_s - \tau)e^{-j2\pi f_c(b(kT_s-\tau)} \ldots.)^\top. \quad (4)$$

The unknown deterministic parameters can be gathered in vector $\boldsymbol{\epsilon}^\top = \left(\sigma_n^2, \rho, \Phi, \boldsymbol{\eta}^\top\right) = \left(\sigma_n^2, \boldsymbol{\theta}^\top\right)$, with $\rho \in \mathbb{R}^+, 0 \leq \Phi \leq 2\pi$. The correctly specified signal model is represented by a probability densitiy function (pdf) denoted $p_{\boldsymbol{\epsilon}}(\mathbf{x};\boldsymbol{\epsilon})$, which follows a complex circular Gaussian distribution $\mathbf{x} \sim \mathcal{CN}\left(\alpha \mathbf{a}(\boldsymbol{\eta}), \sigma_n^2 \boldsymbol{I}_N\right)$.

B. Misspecified Signal Model

The misspecified signal model represents the case where the interference is not considered, i.e., when a mismatched MLE (MMLE) is implemented at the receiver. This nominal case leads to the definition of the misspecified parameter vector $\boldsymbol{\eta}' = [\tau', b']^\top$, and the complete set of unknown parameters $\boldsymbol{\epsilon'}^\top = \left[\sigma_n^2, \rho', \Phi', \boldsymbol{\eta}'^\top\right] = \left[\sigma_n^2, \boldsymbol{\theta}'^\top\right]$, yielding the following signal model at the output of the Hilbert filter,

$$x'(t;\boldsymbol{\eta}') = \alpha' s(t-\tau')e^{-j2\pi f_c b'(t-\tau')} + n(t), \quad (5)$$

with $\alpha' = \rho' e^{j\Phi'}$. Again, we can build the discrete vector signal model from N samples at $T_s = 1/F_s$,

$$\mathbf{x}' = \alpha' \boldsymbol{\mu}(\boldsymbol{\eta}') + \mathbf{n}, \quad (6)$$

with $\boldsymbol{\mu}(\boldsymbol{\eta}') = (\ldots, s(kT_s - \tau')e^{-j2\pi f_c b'(kT_s-\tau')}, \ldots)^\top$. The misspecified signal model is represented by a pdf denoted $f_{\boldsymbol{\epsilon}'}(\mathbf{x};\boldsymbol{\epsilon}')$ which follows a complex circular Gaussian distribution $\mathbf{x}' \sim \mathcal{CN}(\alpha' \boldsymbol{\mu}(\boldsymbol{\eta}'), \sigma_n^2 \boldsymbol{I}_N)$. Note that in this particular scenario, the covariance matrix of the correctly specified signal model equals the covariance matrix of the misspecified signal model, i.e. $\sigma_n^2 \boldsymbol{I}_N$, which does not depend on the synchronization parameters of interest, then:

$$p_{\boldsymbol{\epsilon}}(\mathbf{x};\boldsymbol{\epsilon}) = \frac{1}{\pi^N \sigma_n^{2N}} e^{\frac{-(\mathbf{x}-\alpha \boldsymbol{a}(\boldsymbol{\eta}))^H(\mathbf{x}-\alpha \boldsymbol{a}(\boldsymbol{\eta}))}{\sigma_n^2}}, \quad (7)$$

$$f_{\boldsymbol{\epsilon}'}(\mathbf{x}';\boldsymbol{\epsilon}') = \frac{1}{\pi^N \sigma_n^{2N}} e^{\frac{-(\mathbf{x}-\alpha' \boldsymbol{\mu}(\boldsymbol{\eta}'))^H(\mathbf{x}-\alpha' \boldsymbol{\mu}(\boldsymbol{\eta}'))}{\sigma_n^2}}. \quad (8)$$

Notice that considering the misspecified signal model induces a bias on the corresponding MMLE. These biased estimated parameters are commonly referred to as pseudotrue parameters, $\boldsymbol{\theta}_{pt}^\top = [\rho_{pt}, \Phi_{pt}, \tau_{pt}, b_{pt}]$.

III. Computation of the theoretical MSE

A. Bias Computation via Kullback-Leibler Divergence

The pseudotrue parameters are simply those that give the minimum Kullback-Leibler Divergence (KLD) [15] $D(p_{\boldsymbol{\epsilon}}||f_{\boldsymbol{\epsilon}'}) = E_p\left[\ln p_{\boldsymbol{\epsilon}}(\mathbf{x};\boldsymbol{\epsilon}) - \ln f_{\boldsymbol{\epsilon}'}(\mathbf{x}';\boldsymbol{\epsilon}')\right]$, between the true and assumed models (i.e., because the estimation is independent of σ_n^2), where $E_p[\cdot]$ is the expectation with respect to (w.r.t.) the true model's pdf,

$$\boldsymbol{\theta}_{pt} = \arg\min_{\boldsymbol{\theta}'} \left\{D(p_{\boldsymbol{\epsilon}}||f_{\boldsymbol{\epsilon}'})\right\} = \arg\min_{\boldsymbol{\theta}'} \left\{E_p\left[-\ln f_{\boldsymbol{\epsilon}'}(\mathbf{x};\boldsymbol{\epsilon}')\right]\right\}, \quad (9)$$

In [18] has been shown that in order to compute the parameters that minimizes the KLD, we need to compute the following minimization problem:

$$\arg\min_{\boldsymbol{\theta}'} \left\{\left\|\alpha \boldsymbol{a}(\boldsymbol{\eta}) - \alpha' \boldsymbol{\mu}(\boldsymbol{\eta}')\right\|^2\right\}, \quad (10)$$

where it is simple to show that

$$\left\{\left\|\alpha \boldsymbol{a}(\boldsymbol{\eta}) - \alpha' \boldsymbol{\mu}(\boldsymbol{\eta}')\right\|^2\right\} = \left\|\boldsymbol{\mu}(\boldsymbol{\eta}')\left(\frac{\boldsymbol{\mu}(\boldsymbol{\eta}')^H \alpha \boldsymbol{a}(\boldsymbol{\eta})}{\boldsymbol{\mu}(\boldsymbol{\eta}')^H \boldsymbol{\mu}(\boldsymbol{\eta}')} - \alpha'\right)\right\|^2 + \left\|\alpha \boldsymbol{a}(\boldsymbol{\eta})\right\|^2 - \left\|\Pi_{\boldsymbol{\mu}(\boldsymbol{\eta}')} \alpha \boldsymbol{a}(\boldsymbol{\eta})\right\|^2, \quad (11)$$

with $\Pi_{\mathbf{A}} = \mathbf{A}\left(\mathbf{A}^H\mathbf{A}\right)^{-1}\mathbf{A}^H$. The parameters that minimize the KLD are [18]:

$$\alpha_{pt} = \alpha \frac{\boldsymbol{\mu}(\boldsymbol{\eta}_{pt})^H \boldsymbol{a}(\boldsymbol{\eta})}{\boldsymbol{\mu}(\boldsymbol{\eta}_{pt})^H \boldsymbol{\mu}(\boldsymbol{\eta}_{pt})}, \quad (12)$$

$$\boldsymbol{\eta}_{pt} = \arg\max_{\boldsymbol{\eta}'} \left\{\left\|\Pi_{\boldsymbol{\mu}(\boldsymbol{\eta}')} \alpha \boldsymbol{a}(\boldsymbol{\eta})\right\|^2\right\}, \quad (13)$$

with $\alpha_{pt} = \rho_{pt} e^{j\Phi_{pt}}$ and $\boldsymbol{\eta}_{pt}^\top = [\tau_{pt}, b_{pt}]$. Note that the pseudotrue parameters can be computed with the MMLE without noise. Then, the bias is defined as $\Delta\alpha = \alpha_{pt} - \alpha$, $\boldsymbol{\Delta\eta} = \boldsymbol{\eta}_{pt} - \boldsymbol{\eta}$.

B. Closed-Form MCRB Expressions for a Band-Limited Signal under Interference

In [19], the MCRB was derived as an extension of the Slepian-Bangs formulas, a result that was later expressed as a combination of two information matrices in [15]: $\mathbf{A}(\boldsymbol{\theta}_{pt})$ and $\mathbf{B}(\boldsymbol{\theta}_{pt})$,

$$\mathbf{MCRB}(\boldsymbol{\theta}_{pt}) = \mathbf{A}(\boldsymbol{\theta}_{pt})^{-1}\mathbf{B}(\boldsymbol{\theta}_{pt})\mathbf{A}(\boldsymbol{\theta}_{pt})^{-1}, \quad (14)$$

where

$$\mathbf{A}(\boldsymbol{\theta}_{pt}) = \frac{2}{\sigma_n^2}\Re\left\{(\delta\mathbf{m})^H\left(\frac{\partial^2 \alpha_{pt}\boldsymbol{\mu}(\boldsymbol{\eta}_{pt})}{\partial\boldsymbol{\theta}_{pt}\partial\boldsymbol{\theta}_{pt}^\top}\right)\right\} - \mathbf{B}(\boldsymbol{\theta}_{pt}),$$

$$\mathbf{B}(\boldsymbol{\theta}_{pt}) = \frac{2}{\sigma_n^2}\Re\left\{\left(\frac{\partial \alpha_{pt}\boldsymbol{\mu}(\boldsymbol{\eta}_{pt})}{\partial\boldsymbol{\theta}_{pt}}\right)^H\left(\frac{\partial \alpha_{pt}\boldsymbol{\mu}(\boldsymbol{\eta}_{pt})}{\partial\boldsymbol{\theta}_{pt}}\right)\right\},$$

$\delta\mathbf{m} \triangleq \alpha\mathbf{a}(\boldsymbol{\eta}) - \alpha_{pt}\boldsymbol{\mu}(\boldsymbol{\eta}_{pt}) = \alpha\boldsymbol{\mu}(\boldsymbol{\eta}) + \boldsymbol{I} - \alpha_{pt}\boldsymbol{\mu}(\boldsymbol{\eta}_{pt})$ the mean difference between true and misspecified models.

In $\mathbf{B}(\boldsymbol{\theta}_{pt})$ one can recognize the Fisher Information Matrix (FIM) of a single source CSM. A compact expression of this FIM, that depends only on the baseband signal samples, was recently derived in [10]. We recall hereafter for completeness that

$$\mathbf{B}(\boldsymbol{\theta}_{pt}) = \frac{2F_s}{\sigma_n^2}\Re\left\{\mathbf{Q}\mathbf{W}\mathbf{Q}^H\right\}, \tag{15}$$

with

$$\mathbf{W} = \begin{bmatrix} w_1 & w_2^* & w_3^* \\ w_2 & W_{2,2} & w_4^* \\ w_3 & w_4 & W_{3,3} \end{bmatrix}, \tag{16}$$

$$\mathbf{Q} = \begin{bmatrix} j\alpha_{pt}\omega_c b_{pt} & 0 & -\alpha_{pt} \\ 0 & -j\alpha_{pt}\omega_c & 0 \\ e^{j\Phi_{pt}} & 0 & 0 \\ \alpha_{pt} & 0 & 0 \end{bmatrix}, \tag{17}$$

where the elements of $\mathbf{W}$ can be expressed w.r.t. the baseband signal samples as,

$$w_1 = \frac{1}{F_s}\mathbf{s}^H\mathbf{s}, w_2 = \frac{1}{F_s^2}\mathbf{s}^H\mathbf{D}\mathbf{s},$$
$$w_3 = \frac{1}{F_s}\mathbf{s}^H\mathbf{V}^{\Delta,1}(0)\mathbf{s}, w_4 = \frac{1}{F_s}\mathbf{s}^H\mathbf{D}\mathbf{V}^{\Delta,1}(0)\mathbf{s},$$
$$W_{2,2} = \frac{1}{F_s^3}\mathbf{s}^H\mathbf{D}^2\mathbf{s}, W_{3,3} = F_s\mathbf{s}^H\mathbf{V}^{\Delta,2}(0)\mathbf{s}$$

with $\mathbf{s}$, the baseband samples vector, $\mathbf{D}$, $\mathbf{V}^{\Delta,1}(\cdot)$ and $\mathbf{V}^{\Delta,2}(\cdot)$ defined as,

$$\mathbf{s} = (\ldots, s(nT_s), \ldots)^\top_{N_1\le n\le N_2}, \tag{18}$$
$$\mathbf{D} = \mathrm{diag}(\ldots, n, \ldots)_{N_1\le n\le N_2}, \tag{19}$$
$$\left[\mathbf{V}^{\Delta,1}(q)\right]_{k,l} = \frac{1}{k-l-q}\left(\cos(\pi(k-l-q))\right.$$
$$\left.-\mathrm{sinc}(k-l-q)\right), \tag{20}$$
$$\left[\mathbf{V}^{\Delta,2}(q)\right]_{k,l} = \pi^2\mathrm{sinc}(k-l-q)$$
$$+2\frac{\cos(\pi(k-l-q)) - \mathrm{sinc}(k-l-q)}{(k-l-q)^2}. \tag{21}$$

where the reader can refer to [14] for details on the closed-form expressions of $\mathbf{V}^{\Delta,1}(q)$ and $\mathbf{V}^{\Delta,2}(q)$.

The matrix $\mathbf{A}(\boldsymbol{\theta}_{pt})$ accounts for the model misspecification. Its elements can also be expressed in a compact form as a function of the baseband signal and interference samples as,

$$[\mathbf{A}(\boldsymbol{\theta}_{pt})]_{p,q} = \frac{2F_s}{\sigma_n^2}\Re\left\{[\mathbf{Q}_q]_{p,.}\,\mathbf{W}^{\mathbf{A}}\tilde{\boldsymbol{\alpha}}^*\right\} - [\mathbf{B}(\boldsymbol{\theta}_{pt})]_{p,q},$$
$$\mathbf{W}^{\mathbf{A}} = [\mathbf{w}_1^{\mathbf{A}}\ \mathbf{w}_2^{\mathbf{A}}\ \mathbf{w}_3^{\mathbf{A}}],\ \tilde{\boldsymbol{\alpha}} = \left(\rho e^{j\Phi}, 1, -\rho_{pt}e^{j\Phi_{pt}}\right)^\top, \tag{22}$$

with $\mathbf{w}_1^{\mathbf{A}} = [\ldots, w_{1,l}^{\mathbf{A}}, \ldots]^\top$, $\mathbf{w}_2^{\mathbf{A}} = [\ldots, w_{2,l}^{\mathbf{A}}, \ldots]^\top$ and $\mathbf{w}_3^{\mathbf{A}} = [\ldots, w_{3,l}^{\mathbf{A}}, \ldots]^\top$ for $l \in (1, \cdots, 6)$, and where $[\mathbf{Q}_q]_{p,.}$ is the p-th row of the matrix $\mathbf{Q}_q$ with $q \in (1, \cdots, 4)$ and

$$\mathbf{Q}_1 = \begin{bmatrix} -\alpha_{pt}\omega_c^2 b_{pt}^2 & 0 & 0 & -j2\alpha_{pt}\omega_c b_{pt} & 0 & \alpha_{pt} \\ j\alpha_{pt}\omega_c & \alpha_{pt}\omega_c^2 b_{pt} & 0 & 0 & j\alpha_{pt}\omega_c & 0 \\ je^{j\Phi_{pt}}\omega_c b_{pt} & 0 & 0 & -e^{j\Phi_{pt}} & 0 & 0 \\ -\alpha_{pt}\omega_c b_{pt} & 0 & 0 & -j\alpha_{pt} & 0 & 0 \end{bmatrix}, \tag{23}$$

$$\mathbf{Q}_2 = \begin{bmatrix} j\alpha_{pt}\omega_c & \alpha_{pt}\omega_c^2 b_{pt} & 0 & 0 & j\alpha_{pt}\omega_c & 0 \\ 0 & 0 & -\alpha_{pt}\omega_c^2 & 0 & 0 & 0 \\ 0 & -je^{j\Phi_{pt}}\omega_c & 0 & 0 & 0 & 0 \\ 0 & \alpha_{pt}\omega_c & 0 & 0 & 0 & 0 \end{bmatrix}, \tag{24}$$

$$\mathbf{Q}_3 = \begin{bmatrix} je^{j\Phi_{pt}}\omega_c b_{pt} & 0 & 0 & -e^{j\Phi_{pt}} & 0 & 0 \\ 0 & -je^{j\Phi_{pt}}\omega_c & 0 & 0 & 0 & 0 \\ 0 & 0 & 0 & 0 & 0 & 0 \\ je^{j\Phi_{pt}} & 0 & 0 & 0 & 0 & 0 \end{bmatrix}, \tag{25}$$

$$\mathbf{Q}_4 = \begin{bmatrix} -\alpha_{pt}\omega_c b_{pt} & 0 & 0 & -j\alpha_{pt} & 0 & 0 \\ 0 & \alpha_{pt}\omega_c & 0 & 0 & 0 & 0 \\ je^{j\Phi_{pt}} & 0 & 0 & 0 & 0 & 0 \\ -\alpha_{pt} & 0 & 0 & 0 & 0 & 0 \end{bmatrix}, \tag{26}$$

Finally: $\Delta\tau = \tau - \tau_{pt}$ and $\Delta b = b - b_{pt}$, and $\mathbf{W}^{\mathbf{A}}$ is obtained from,

$$w_{1,1}^{\mathbf{A}}(\boldsymbol{\eta})^* = \frac{1}{F_s}\mathbf{s}^H\mathbf{U}\left(\frac{f_c\Delta b}{F_s}\right)\mathbf{V}^{\Delta,0}\left(\frac{\Delta\tau}{T_s}\right)\mathbf{s}\,e^{j\omega_c b\Delta\tau},, \tag{27}$$

$$w_{1,2}^{\mathbf{A}}(\boldsymbol{\eta})^* = \frac{1}{F_s^2}\mathbf{s}^H\mathbf{D}\mathbf{U}\left(\frac{f_c\Delta b}{F_s}\right)\mathbf{V}^{\Delta,0}\left(\frac{\Delta\tau}{T_s}\right)\mathbf{s}\,e^{j\omega_c b\Delta\tau}, \tag{28}$$

$$w_{1,3}^{\mathbf{A}}(\boldsymbol{\eta})^* = \frac{1}{F_s^3}\mathbf{s}^H\mathbf{D}^2\mathbf{U}\left(\frac{f_c\Delta b}{F_s}\right)\mathbf{V}^{\Delta,0}\left(\frac{\Delta\tau}{T_s}\right)\mathbf{s}\,e^{j\omega_c b\Delta\tau}, \tag{29}$$

$$w_{1,4}^{\mathbf{A}}(\boldsymbol{\eta})^* = \left(-\mathbf{s}^H\mathbf{U}\left(\frac{f_c\Delta b}{F_s}\right)\mathbf{V}^{\Delta,1}\left(\frac{\Delta\tau}{T_s}\right)\mathbf{s}+\right.$$
$$\left.\frac{j\omega_c\Delta b}{F_s}\mathbf{s}^H\mathbf{U}\left(\frac{f_c\Delta b}{F_s}\right)\mathbf{V}^{\Delta,0}\left(\frac{\Delta\tau}{T_s}\right)\mathbf{s}\right).e^{j\omega_c b\Delta\tau}, \tag{30}$$

$$w_{1,5}^{\mathbf{A}}(\boldsymbol{\eta})^* = \left(-\frac{1}{F_s}\mathbf{s}^H\mathbf{U}\left(\frac{f_c\Delta b}{F_s}\right)\mathbf{V}^{\Delta,0}\left(\frac{\Delta\tau}{T_s}\right)\mathbf{s}\right.$$
$$-\frac{1}{F_s}\mathbf{s}^H\mathbf{D}\mathbf{U}\left(\frac{f_c\Delta b}{F_s}\right)\mathbf{V}^{\Delta,1}\left(\frac{\Delta\tau}{T_s}\right)\mathbf{s}$$
$$\left.+j\frac{\omega_c\Delta b}{F_s^2}\mathbf{s}^H\mathbf{D}\mathbf{U}\left(\frac{f_c\Delta b}{F_s}\right)\mathbf{V}^{\Delta,0}\left(\frac{\Delta\tau}{T_s}\right)\mathbf{s}\right)\,e^{j\omega_c b\Delta\tau}, \tag{31}$$

$$w_{1,6}^{\mathbf{A}}(\boldsymbol{\eta})^* = \left(-F_s\mathbf{s}^H\mathbf{U}\left(\frac{f_c\Delta b}{F_s}\right)\mathbf{V}^{\Delta,2}\left(\frac{\Delta\tau}{T_s}\right)\mathbf{s}\right.$$
$$-j2\omega_c\Delta b\mathbf{s}^H\mathbf{U}\left(\frac{f_c\Delta b}{F_s}\right)\mathbf{V}^{\Delta,1}\left(\frac{\Delta\tau}{T_s}\right)\mathbf{s}$$
$$\left.-\frac{(\omega_c\Delta b)^2}{F_s}\mathbf{s}^H\mathbf{U}\left(\frac{f_c\Delta b}{F_s}\right)\mathbf{V}^{\Delta,0}\left(\frac{\Delta\tau}{T_s}\right)\mathbf{s}\right)\,e^{j\omega_c b\Delta\tau}, \tag{32}$$

$$w_{2,1}^{\mathbf{A}} = \frac{1}{F_s}\mathbf{I}^H\mathbf{V}^{\Delta,0}\left(\frac{\tau_{pt}}{T_s}\right)\mathbf{U}\left(\frac{f_c b_{pt}}{F_s}\right)\mathbf{s}, \tag{33}$$

$$w_{2,2}^{\mathbf{A}} = \frac{1}{F_s^2}\mathbf{I}^H\mathbf{V}^{\Delta,0}\left(\frac{\tau_{pt}}{T_s}\right)\mathbf{U}\left(\frac{f_c b_{pt}}{F_s}\right)\mathbf{D}\mathbf{s}, \tag{34}$$

$$w_{2,3}^{\mathbf{A}} = \frac{1}{F_s^3}\mathbf{I}^H\mathbf{V}^{\Delta,0}\left(\frac{\tau_{pt}}{T_s}\right)\mathbf{U}\left(\frac{f_c b_{pt}}{F_s}\right)\mathbf{D}^2\mathbf{s}, \tag{35}$$

$$w_{2,4}^{\mathbf{A}} = \mathbf{I}^H \mathbf{V}^{\Delta,1}\left(\frac{\tau_{pt}}{T_s}\right)\mathbf{U}\left(\frac{f_c b_{pt}}{F_s}\right)\mathbf{s} + \frac{j\omega_c b_{pt}}{F_s}\mathbf{I}^H \mathbf{V}^{\Delta,0}\left(\frac{\tau_{pt}}{T_s}\right)\mathbf{U}\left(\frac{f_c b_{pt}}{F_s}\right)\mathbf{s}, \quad (36)$$

$$w_{2,5}^{\mathbf{A}} = -\frac{1}{F_s}\mathbf{I}^H \mathbf{V}^{\Delta,0}\left(\frac{\tau_{pt}}{T_s}\right)\mathbf{U}\left(\frac{f_c b_{pt}}{F_s}\right)\mathbf{s} + \frac{1}{F_s}\mathbf{I}^H \mathbf{V}^{\Delta,1}\left(\frac{\tau_{pt}}{T_s}\right)\mathbf{U}\left(\frac{f_c b_{pt}}{F_s}\right)\mathbf{D}\mathbf{s} + j\frac{\omega_c b_{pt}}{F_s^2}\mathbf{I}^H \mathbf{V}^{\Delta,0}\left(\frac{\tau_{pt}}{T_s}\right)\mathbf{U}\left(\frac{f_c b_{pt}}{F_s}\right)\mathbf{D}\mathbf{s}, \quad (37)$$

$$w_{2,6}^{\mathbf{A}} = -F_s \mathbf{I}^H \mathbf{V}^{\Delta,2}\left(\frac{\tau_{pt}}{T_s}\right)\mathbf{U}\left(\frac{f_c b_{pt}}{F_s}\right)\mathbf{s} + j2\omega_c b_{pt}\mathbf{I}^H \mathbf{V}^{\Delta,1}\left(\frac{\tau_{pt}}{T_s}\right)\mathbf{U}\left(\frac{f_c b_{pt}}{F_s}\right)\mathbf{s} - \frac{(\omega_c b_{pt})^2}{F_s}\mathbf{I}^H \mathbf{V}^{\Delta,0}\left(\frac{\tau_{pt}}{T_s}\right)\mathbf{U}\left(\frac{f_c b_{pt}}{F_s}\right)\mathbf{s}, \quad (38)$$

$$w_{3,1}^{\mathbf{A}} = w_1,\ w_{3,2}^{\mathbf{A}} = w_2,\ w_{3,3}^{\mathbf{A}} = W_{2,2}, \quad (39)$$

$$w_{3,4}^{\mathbf{A}} = w_3,\ w_{3,5}^{\mathbf{A}} = w_4,\ w_{3,6}^{\mathbf{A}} = -W_{3,3}. \quad (40)$$

with

$$\mathbf{U}(p) = \text{diag}\left(\ldots, e^{-j2\pi pn}, \ldots\right)_{N_1 \le n \le N_2}, \quad (41)$$

$$\left[\mathbf{V}^{\Delta,0}(q)\right]_{k,l} = \text{sinc}\left(k - l - q\right) \quad (42)$$

The entire derivation can be found in [14]. However, the equations included above are self-contained and it is not necessary to go to the proof to perform the implementation.

IV. Results

Let us consider the case where a L5/E5a GNSS signal is interfered by a DME system. The signal transmitted by an individual DME station is composed of a pair of Gaussian pulses, modulated by a cosine, at central frequency f_{DME}. The interference baseband signal at the output of the receiver's Hilbert filter can be modeled as:

$$I(t) = \sum_{i=1}^{K} I_i \cdot \left(e^{-\frac{\gamma(t-t_i)^2}{2}} + e^{-\frac{\gamma(t-t_i-\delta_t)^2}{2}}\right) e^{-j2\pi(f_i)t}, \quad (43)$$

with I_i a complex gain whose module represents the received interference beacon peak power of the i-th pulse pair, $\gamma = 4.5 \cdot 10^{11} s^{-2}$, $\delta_t = 12\mu s$, t_i represents the i-th pulse pair reception time, and f_i the received frequency of the i-th pulse pair after the baseband demodulation process, i.e., $f_i = f_{DME_i} - f_c + f_{D_i}$, where f_{DME_i} is the central frequency of the transmitted i-th pulse pair, f_c the central frequency of the L5/E5a GNSS signal, and f_{D_i} is the Doppler frequency associated to the reception of the i-th pulse pair. Finally, K is the number of pulse pairs received within the GNSS signal integration period.

We underline that the aircraft's DME interrogators transmitting their signals between 1025 MHz and 1150 MHz are ignored herein. This study focuses on DME ground stations/repeaters, as they transmit their signals between 962 MHz and 1213 MHz, which includes the L5/E5a GNSS band of interest (i.e., between 1164 MHz and 1191 MHz). The band is divided into 126 channels for interrogation and 126 channels for reply. The interrogation and reply frequencies always differ by 63 MHz. The spacing among channels is 1 MHz.

The following scenario is proposed to verify the theory introduced in Section III. We consider 7 DME signals interfering the GNSS receiver, with $f_i = [-0.5, -0.25, 0.15, 0, 0.15, 0.25, 0.5]$ MHz, and arriving at the receiver $[1.25, 2.5, 3.75, 5, 6.25, 7.5, 8.75]$ ms after the first chip of the GNSS PRN code. We consider the reception of a GPS L5Q signal. The integration time is set to 10 ms. The ambiguity function without interference is illustrated in Figure 1.

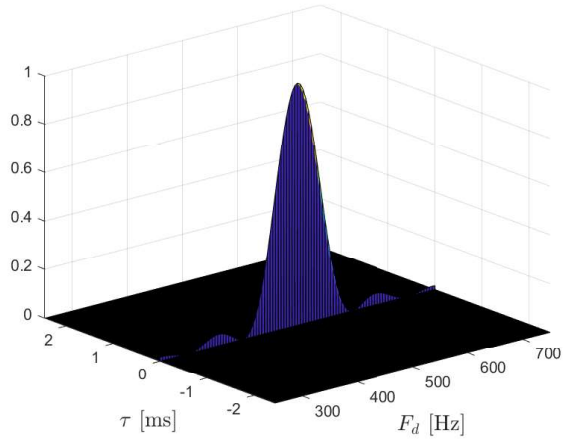

Fig. 1. Ambiguity function of the GPS L5Q signal. The integration time is set to 10 ms, $F_s = 20$ MHz.

The ambiguity function for the GNSS+DME scenario described above, for a pulse power $I_i = 30$dB, is shown in Figure 2. It is interesting to check that even if there are extra secondary lobes due to the DME signals, the main GPS L5Q lobe apparently does not change in position or shape. The same effect can be seen in Figure 3, where $I_i = 32$dB.

For these two cases, $I_i = \{30, 32\}$dB, Figures 4 - 7 show the MSE and bias for the parameters of interest $\boldsymbol{\eta}^T$ w.r.t. the SNR at the output of the matched filter (i.e., SNR_{OUT}), obtained from 1000 Monte Carlo runs. In these results one can observe that: i) the root MSE ($\sqrt{MSE}$) of the true parameter converges to $\sqrt{MCRB + Bias^2}$, ii) the $\sqrt{MSE}$ of the pseudotrue parameter converges to the $\sqrt{MCRB}$, and iii) the $\sqrt{CRB}$ represents the asymptotic estimation performance without any source of interference. Such results validate and prove the exactness of the proposed MCRB and bias expressions. Interestingly, while the other parameter estimates (i.e., Doppler, amplitude and phase) are biased, in Figure 4 one can observe that the time-delay MSE almost (i.e., the MCRB is slightly larger than the CRB) converges asymptotically to the case without interference, and then the time-delay MLE is almost asymptotically unbiased. However, increasing the

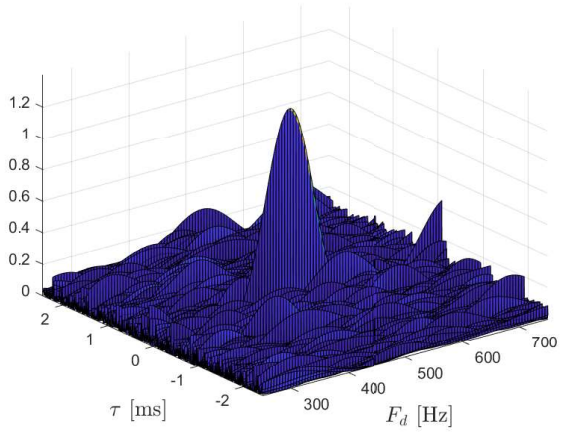

Fig. 2. Ambiguity function of the GPS L5Q signal. The integration time is set to 10 ms, $F_s = 20$ MHz. $I_i = 30$dB.

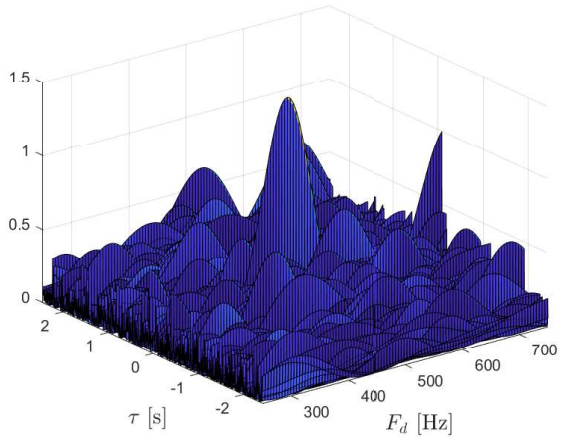

Fig. 3. Ambiguity function of the GPS L5Q signal. The integration time is set to 10 ms, $F_s = 20$ MHz. $I_i = 32$dB.

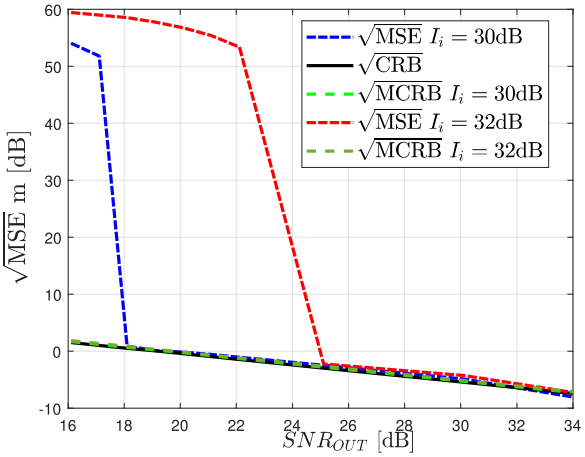

Fig. 4. RMSE of the time-delay of the GPS L5Q signal. The integration time is set to 10 ms, $F_s = 20$ MHz and $I_i = \{30, 32\}$dB.

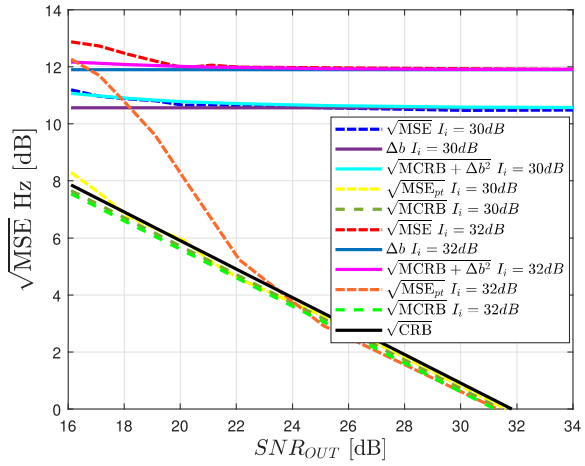

Fig. 5. RMSE of the Doppler of the GPS L5Q signal. The integration time is set to 10 ms, $F_s = 20$ MHz and $I_i = \{30, 32\}$dB.

interference power has an efect in the convergence threshold of the MLE to the corresponding asymptotical performance.

Finally, the ambiguity function when $I_i = 34$ dB is shown in Figure 8. Note that under this particular scenario (i.e., and for pulse powers larger than this value) the MLE does not converge anymore, since the power of the DME signal completely masks the GNSS L5Q signal: GNSS breakdown.

V. Conclusion

It is well documented in the literature that interference signals may have a huge impact on the GNSS receivers' performance, but to the best of the authors' knowledge, from an estimation perspective, the theoretical analysis of the impact of such intereferences on the first GNSS receiver stage (i.e., time-delay and Doppler estimation) is an important missing point. In practice, at the receiver there exists a model mismatch, and an interference induces both i) an estimation bias and ii) a variance degradation. In this contribution, we provided the theoretical closed-form expressions that characterize the MSE for the MLE of the GNSS synchronization parameters, that is, bias and MCRB. Comparing these results to the standard CRB, associated to the unbiased MLE without any interference, allows to theoretically characterize the performance degradation on the time-delay and Doppler estimation. The exactness of the proposed expressions was validated for a representative case where a DME system interfere a GNSS L5/E5a signal. Results were provided to show such validity and the impact on both time-delay and Doppler estimation. It is important to notice that such analysis may allow to design robust metrics for the design of new GNSS signals, as well as the design of new interference countermeasures.

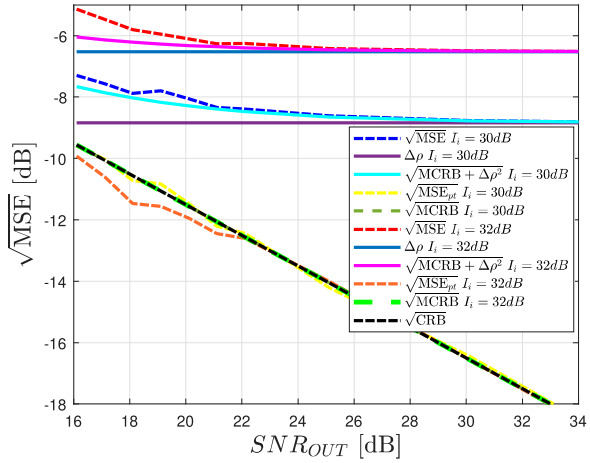

Fig. 6. RMSE of the amplitude ρ of the GPS L5Q signal. The integration time is set to 10 ms, $F_s = 20$ MHz and $I_i = \{30, 32\}$dB.

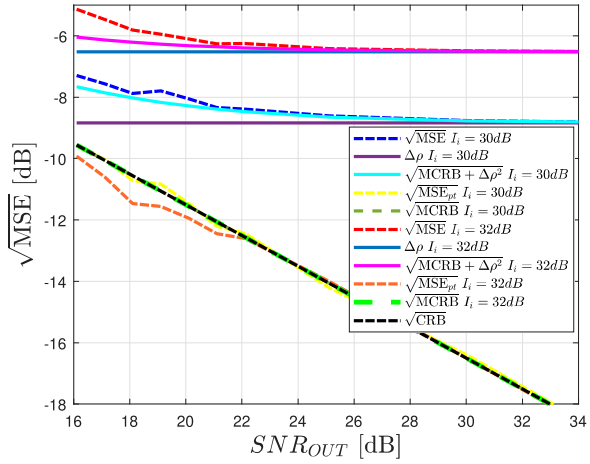

Fig. 7. RMSE of the phase ϕ of the GPS L5Q signal. The integration time is set to 10 ms, $F_s = 20$ MHz and $I_i = \{30, 32\}$dB.

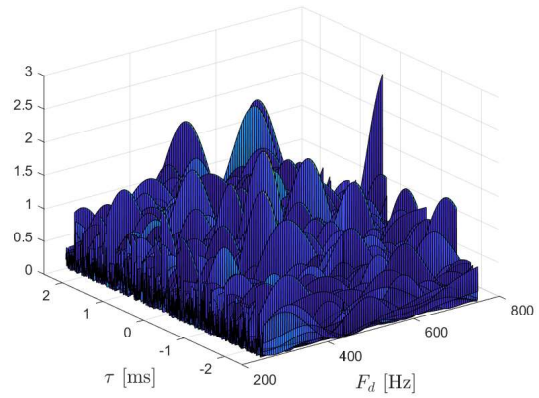

Fig. 8. Ambiguity function of the GPS L5Q signal. The integration time is set to 10 ms, $F_s = 20$ MHz. $I_i = 34$dB.

ACKNOWLEDGMENT

This work has been partially supported by the DGA/AID projects 2022.65.0082, 2021.65.0070.00.470.75.01, and TéSA.

REFERENCES

[1] P. J. G. Teunissen and O. Montenbruck, Eds., *Handbook of Global Navigation Satellite Systems*. Switzerland: Springer, 2017.

[2] M. G. Amin, P. Closas, A. Broumandan, and J. L. Volakis, "Vulnerabilities, Threats, and Authentication in Satellite-Based Navigation Systems [scanning the issue]," *Proceedings of the IEEE*, vol. 104, no. 6, pp. 1169–1173, June 2016.

[3] R. Morales-Ferre, P. Richter, E. Falletti, A. de la Fuente, and E. S. Lohan, "A Survey on Coping With Intentional Interference in Satellite Navigation for Manned and Unmanned Aircraft," *IEEE Commun. Surv. Tutor.*, vol. 22, no. 1, pp. 249–291, 2020.

[4] C. Fernández-Prades, J. Arribas, and P. Closas, "Robust GNSS Receivers by Array Signal Processing: Theory and Implementation," *Proceedings of the IEEE*, vol. 104, no. 6, pp. 1207–1220, June 2016.

[5] M. G. Amin, D. Borio, Y. D. Zhang, and L. Galleani, "Time-Frequency Analysis for GNSSs: From Interference Mitigation to System Monitoring," *IEEE Signal Process. Mag.*, vol. 34, no. 5, pp. 85–95, 2017.

[6] J. Arribas, J. Vilà-Valls, A. Ramos, C. Fernández-Prades, and P. Closas, "Air Traffic Control Radar Interference in the Galileo E6 Band: Detection and Localization," *Navigation*, vol. 66, no. 3, pp. 505–522, 2019.

[7] D. Borio and C. Gioia, "GNSS Interference Mitigation: A Measurement and Position Domain Assessment," *Navigation*, vol. 68, no. 1, pp. 93–114, 2021.

[8] G. X. Gao, L. Heng, A. Hornbostel, H. Denks, M. Meurer, T. Walter, and P. Enge, "Dme/tacan interference mitigation for gnss: algorithms and flight test results," *GPS solutions*, vol. 17, no. 4, pp. 561–573, 2013.

[9] A. Renaux, P. Forster, E. Chaumette, and P. Larzabal, "On the High-SNR Conditional Maximum-Likelihood Estimator Full Statistical Characterization," *IEEE Trans. Signal Process.*, vol. 54, no. 12, pp. 4840 – 4843, Dec. 2006.

[10] D. Medina, L. Ortega, J. Vilà-Valls, P. Closas, F. Vincent, and E. Chaumette, "Compact CRB for Delay, Doppler and Phase Estimation - Application to GNSS SPP & RTK Performance Characterization," *IET Radar, Sonar & Navigation*, vol. 14, no. 10, pp. 1537–1549, Sep. 2020.

[11] C. Lubeigt, L. Ortega, J. Vilà-Valls, L. Lestarquit, and E. Chaumette, "Joint Delay-Doppler Estimation Performance in a Dual Source Context," *Remote Sensing*, vol. 12, no. 23, 2020. [Online]. Available: https://www.mdpi.com/2072-4292/12/23/3894

[12] H. McPhee, L. Ortega, J. Vilà-Valls, and E. Chaumette, "Accounting for acceleration - signal parameters estimation performance limits in high dynamics applications," *IEEE Transactions on Aerospace and Electronic Systems*, pp. 1–13, 2022.

[13] C. Lubeigt, L. Ortega, J. Vilà-Valls, and E. Chaumette, "Untangling first and second order statistics contributions in multipath scenarios," *Signal Processing*, vol. 205, p. 108868, 2023.

[14] L. Ortega, C. Lubeigt, J. Vilà-Valls, and E. Chaumette, "On the GNSS Synchronization Performance Degradation under Interference Scenarios: Bias and Misspecified CRB," *Navigation, Under review*, 2023.

[15] S. Fortunati, F. Gini, M. S. Greco, and C. D. Richmond, "Performance Bounds for Parameter Estimation under Misspecified Models: Fundamental Findings and Applications," *IEEE Signal Process. Mag.*, vol. 34, no. 6, pp. 142–157, 2017.

[16] A. Dogandzic and A. Nehorai, "Cramér-Rao Bounds for Estimating Range, Velocity, and Direction with an Active Array," *IEEE Trans. Signal Process.*, vol. 49, no. 6, pp. 1122–1137, June 2001.

[17] M. I. Skolnik, *Radar Handbook*, 3rd ed. New York, USA: McGraw-Hill, 1990.

[18] L. Ortega, J. Vilà-Valls, and E. Chaumette, "Theoretical evaluation of the gnss synchronization performance degradation under interferences," Denver, CO, USA, Sep. 2022.

[19] C. D. Richmond and L. L. Horowitz, "Parameter Bounds on Estimation Accuracy Under Model Misspecification," *IEEE Trans. Signal Process.*, vol. 63, no. 9, pp. 2263–2278, 2015.